# Transport Coefficients of Helical Wormlike Chains. 3. Intrinsic Viscosity†

**Hiromi Yamakawa* and Takenao Yoshizaki**

*Department of Polymer Chemistry, Kyoto University, Kyoto, Japan.*
*Received November 6, 1979*

ABSTRACT: The intrinsic viscosity of the helical wormlike chain is evaluated by an application of the Oseen–Burgers procedure of hydrodynamics to the cylinder model with the preaveraged Oseen tensor. The end effect is however taken into account in such a way that as the chain length is decreased, the Oseen–Burgers solution for the long chain joins with the exact solution obtained previously for the spheroid-cylinder, i.e., a straight cylinder with oblate, spherical, or prolate hemispheroid caps at the ends. The numerical solutions of the integral equation are obtained by means of effective maneuvers. A useful empirical interpolation formula is also presented to be valid for arbitrary contour length and for any possible values of the model parameters. Some salient aspects of the behavior of the intrinsic viscosity are then discussed on the basis of the numerical results. Finally, an analysis of experimental data is made for the intrinsic viscosity, sedimentation coefficient, and mean-square radius of gyration for poly(phthaloyl-*trans*-2,5-dimethylpiperazine) (PPDP), poly(terephthaloyl-*trans*-2,5-dimethylpiperazine) (PTDP), cellulose acetate, and amylose. It is concluded that PPDP, cellulose acetate, and amylose in dimethyl sulfoxide may be represented by the helical wormlike chains, but PTDP may be represented by the ordinary wormlike chain.

In a previous paper,[1] part 2 of this series, we evaluated the translational friction (or diffusion) coefficient of the helical wormlike (HW) chain[2,3] by an application of the Oseen–Burgers (OB) procedure of hydrodynamics to the cylinder model. In this paper, we proceed to evaluate the intrinsic viscosity along the same line but with a consideration of the end effect. Thus, its object is also to analyze transport data for several stiff chain macromolecules to show that some of them may be better represented by the HW chains rather than by the ordinary Kratky–Porod (KP) wormlike chains.[4]

The evaluation is carried out with the preaveraged Oseen hydrodynamic interaction tensor as in the case of the translational friction coefficient[1] (and also of KP chains[4]), so that the coupling between translational and rotational motions[5] need not be considered. Even in this approximation, the solution for the intrinsic viscosity cannot be obtained analytically, and moreover, the numerical solutions are not accessible for short chains, as already seen in the case of KP chains.[4] On the other hand, the OB procedure itself in general is valid only for long enough cylinders. This is the reason why the end effect was not considered at all from the start in the previous treatments. In order to examine the validity of this procedure and the end effect, especially for short cylinders, we have recently evaluated numerically the transport coefficients of straight spheroid-cylinders, i.e., cylinders with oblate or prolate hemispheroid caps at the ends (including spherocylinders), by an orthodox method of classical hydrodynamics.[6] (Note that Norisuye et al.[7] have evaluated the translational friction coefficient of KP spherocylinders by the OB procedure.) The results show that the end effects on the translational and rotatory diffusion coefficients are rather small, while the effect on the intrinsic viscosity is remarkable, depending on the shape of the ends, though for relatively short cylinders. For practical purposes, therefore, we make an attempt to construct empirical interpolation formulas for the intrinsic viscosity on the basis of the solutions for short spheroid-cylinders and those for long HW chains (including KP chains).

The plan of the present paper is as follows. In the next section, we present necessary basic equations. Before obtaining the OB numerical solutions, we first construct an empirical interpolation formula for the intrinsic viscosity of associated KP chains[1,3] along the line mentioned above. Then, the numerical solutions are obtained for the ratio of the intrinsic viscosity of HW chains to that of associated KP chains by means of maneuvers. We also construct an interpolation formula for this ratio and show some salient aspects of the behavior of the intrinsic viscosity of HW chains. Finally, we make an analysis of experimental data for the intrinsic viscosity, sedimentation coefficient, and mean-square radius of gyration for poly(phthaloyl-*trans*-2,5-dimethylpiperazine), poly(terephthaloyl-*trans*-2,5-dimethylpiperazine), cellulose acetate, and amylose.

## Basic Equations

As before,[1-3] we consider the HW chain as an elastic wire with vanishing Poisson's ratio $\sigma$, so that its equilibrium average configuration for a given contour length may be described by three parameters: the constant curvature $\kappa_0$ and constant torsion $\tau_0$ of the characteristic helix and the stiffness parameter $\lambda^{-1}$. It is sometimes convenient to use instead of $\kappa_0$ and $\tau_0$ the parameters defined by[1]

$$\mu = \tau_0(\kappa_0^2 + \tau_0^2)^{-1/2} \qquad \nu = (\kappa_0^2 + \tau_0^2)^{1/2} \tag{1}$$

Ignoring the end effect for the moment within the framework of the OB procedure, we consider the HW cylinder of length $L$ and diameter $d$ as the hydrodynamic model. In what follows, all lengths are measured in units of $\lambda^{-1}$ unless specified otherwise.

Now, suppose that the cylinder is immersed in a steady shear flow of solvent. In the OB approximation, the Newtonian zero-frequency intrinsic viscosity $[\eta]$ may be evaluated from[4]

$$[\eta] = (N_A L/M)\int_{-1}^{1}\psi(x,x)\,dx \tag{2}$$

where $N_A$ is the Avogadro number, $M$ is the molecular weight of the cylinder, and $\psi(x,y)$ is the solution of the integral equation,

$$\int_{-1}^{1}K(x,\xi)\psi(\xi,y)\,d\xi = g(x,y) \tag{3}$$

The kernel $K$ and the known part $g$ are related to the equilibrium average quantities $\langle\ \rangle$,

† This paper is contributed to the celebration of the 70th birthday of Professor Paul J. Flory in recognition of his pioneering and lasting contributions to polymer science.

0024-9297/80/2213-0633$01.00/0 

$$K(x,y) = \langle |\mathbf{R} - \mathbf{r}|^{-1} \rangle \tag{4}$$

$$g(x,y) = (\pi/L)\langle \mathbf{S}(s)\cdot\mathbf{S}(s') \rangle \tag{5}$$

with

$$x = (2s/L) - 1 \qquad y = (2s'/L) - 1 \tag{6}$$

where $\mathbf{R} = \mathbf{R}(s,s')$ is the vector distance between the contour points $s$ and $s'$ ($0 \le s,s' \le L$), $\mathbf{r}$ is the normal radius vector from the contour point $s$ to the cylinder surface so that $|\mathbf{r}| = d/2$, $\mathbf{S}(s)$ is the vector distance from the molecular center of mass to the contour point $s$, and in eq 4 the $\langle\ \rangle$ denotes not only the configurational average but also the average over $\mathbf{r}$.

The mean reciprocal distance in eq 4 has already been obtained as[1,8]

$$K(x,y) = (t^2 + \tfrac{1}{4}d^2)^{-1/2}\left(1 + \sum_{j=1}^{5} f_{j0}t^j + \sum_{j=1}^{3}\sum_{k=1}^{2} f_{jk}d^{2k}t^j\right) \qquad \text{for } t \le \sigma_1$$

$$K(x,y) = (6/\pi c_\infty t)^{1/2}\sum_{j=0}^{2}\sum_{k=0}^{j} B_{jk}d^{2k}(c_\infty t)^{-j} + h(\sigma_2 - t)(c_\infty t)^{-1/2}\sum_{j=0}^{q}\sum_{k=0}^{2} E_{jk}d^{2k}(t - \sigma_2)^{j+3} \qquad \text{for } t > \sigma_1 \tag{7}$$

with

$$t = \tfrac{1}{2}L|x - y| = |s - s'| \tag{8}$$

$$f_{10} = \tfrac{1}{3} \qquad B_{00} = 1 \qquad B_{11} = -0.125 \qquad B_{22} = 0.0140625 \tag{9}$$

where $h(x)$ is the unit step function defined by $h(x) = 1$ for $x \ge 0$ and $h(x) = 0$ for $x < 0$, and $\sigma_1$, $\sigma_2$, $f_{j0}$ ($j$ = 2–5), $f_{jk}$ ($j$ = 1–3; $k$ = 1,2), $B_{10}$, $B_{20}$, $B_{21}$, $E_{jk}$, and $q$ are constants independent of $t$ and $d$ but dependent on $\kappa_0$ and $\tau_0$ and will be determined numerically to give a good approximation to $K(x,y)$ (for the details, see ref 8). $c_\infty$ is the Kuhn segment length of the HW chain (with Poisson's ratio $\sigma$ = 0) and is given by

$$c_\infty = \lim_{L\to\infty}(\langle R^2\rangle/L) = \frac{4 + \tau_0^2}{4 + \kappa_0^2 + \tau_0^2} = \frac{4 + \mu^2\nu^2}{4 + \nu^2} \qquad (\sigma = 0) \tag{10}$$

with $\langle R^2 \rangle$ the mean-square end-to-end distance of the chain (of contour length $L$).

The average of the scalar product in eq 5 may be evaluated from

$$\langle \mathbf{S}(s)\cdot\mathbf{S}(s') \rangle = \frac{1}{2L}\left[\int_0^L \langle R^2(s,s')\rangle\, ds + \int_0^L \langle R^2(s,s')\rangle\, ds'\right] - \frac{1}{2}\langle R^2(s,s')\rangle - \langle S^2\rangle \tag{11}$$

where $\langle S^2 \rangle$ is the mean-square radius of gyration of the chain (of contour length $L$) and is given by eq 56 of ref 2 with $t = L$ and $\sigma = 0$; $\langle R^2(s,s') \rangle$ is given by eq 54 of ref 2 with $t = |s - s'|$ and $\sigma = 0$. For later use, it is convenient to give the explicit expression for the former,

$$\langle S^2 \rangle = \mu^2\langle S^2\rangle_{KP} + (1 - \mu^2)\left[\frac{L}{3r}\cos\phi - \frac{1}{r^2}\cos(2\phi) + \frac{2}{r^3 L}\cos(3\phi) - \frac{2}{r^4L^2}\cos(4\phi) + \frac{2}{r^4L^2}e^{-2L}\cos(\nu L + 4\phi)\right] \qquad (\sigma = 0) \tag{12}$$

where

$$r = (4 + \nu^2)^{1/2} \tag{13}$$

$$\phi = \cos^{-1}(2/r) \tag{14}$$

and $\langle S^2 \rangle_{KP}$ is the $\langle S^2 \rangle$ of the KP chain with the same $\lambda^{-1}$ as that of the HW chain under consideration and is given by

$$\langle S^2 \rangle_{KP} = \frac{L}{6} - \frac{1}{4} + \frac{1}{4L} - \frac{1}{8L^2}(1 - e^{-2L}) \tag{15}$$

(Note that eq 15 has been derived originally by Benoit and Doty.[9]) Thus, we obtain, from eq 5, 11, and 12,

$$g(x,y) = \frac{\pi}{8L^2}\left\{c_\infty L^2\left(x^2 + y^2 - 2|x - y| + \frac{2}{3}\right) - 8\sum_{j=1}^{3}\frac{c_j}{z_j}e^{-z_jL/2}[\cosh(\tfrac{1}{2}z_jLx) + \cosh(\tfrac{1}{2}z_jLy)] - 4L\sum_{j=1}^{3}c_j e^{-z_jL|x-y|/2} + 8\sum_{j=1}^{3}\frac{c_j}{z_j}\left[1 + \frac{1}{z_jL}(1 - e^{-z_jL})\right]\right\} \tag{16}$$

with

$$c_1 = \tfrac{1}{2}\mu^2 \qquad c_2 = c_3^* = (1 - \mu^2)r^{-4}(4 - \nu^2 - 4i\nu) \tag{17}$$

$$z_1 = 2 \qquad z_2 = z_3^* = 2 + i\nu \tag{18}$$

where $r$ is defined by eq 13, $i$ is the imaginary unit, and the asterisk indicates the complex conjugate.

Before proceeding to calculate the intrinsic viscosity of the HW chain from eq 2 and 3, in the next section we consider the intrinsic viscosity $[\eta]_{a\text{-}KP}$ of the associated KP chain, i.e., the KP chain whose Kuhn segment length is equal to $c_\infty$.

## The Associated KP Chain

An expression for any average quantity for the associated KP chain may be obtained from the corresponding expression for the KP chain by replacing all (reduced) lengths $l$ by $c_\infty^{-1}l$. As given in part 2, therefore, the kernel $K_{a\text{-}KP}(t,d)$ as a function of $t$ (defined by eq 8) and $d$ for the associated KP chain may be expressed in terms of the kernel $K_{KP}(t,d)$ for the KP chain as

$$K_{a\text{-}KP}(t,d) = c_\infty^{-1}K_{KP}(c_\infty^{-1}t, c_\infty^{-1}d) \tag{19}$$

Equation 19 with eq 24 of ref 4 gives the result identical with that given by eq 7 with the $\sigma_1$, $f_{j0}$ ($j$ = 1–5), $f_{jk}$ ($j$ = 1–3; $k$ = 1,2), $B_{10}$, $B_{20}$, and $B_{21}$ given by eq 26 of part 2 and with $\sigma_2 = \sigma_1$ and $E_{jk} = q = 0$. Further, we have

$$\langle \mathbf{S}(s)\cdot\mathbf{S}(s') \rangle_{a\text{-}KP} = c_\infty^2\langle \mathbf{S}(c_\infty^{-1}s)\cdot\mathbf{S}(c_\infty^{-1}s') \rangle_{KP} \tag{20}$$

so that the known part $g_{a\text{-}KP}(x,y)$ in the integral eq 3 for the associated KP chain may be obtained, from eq 5 and 20 with eq 19 of ref 4, as

$$g_{a\text{-}KP}(x,y) = \frac{\pi}{8L^2}\left\{c_\infty L^2\left(x^2 + y^2 - 2|x - y| + \frac{2}{3}\right) - 2c_\infty^2 L e^{-L|x-y|/c_\infty} - 2c_\infty^3 e^{-L/c_\infty}\left[\cosh\left(\frac{Lx}{c_\infty}\right) + \cosh\left(\frac{Ly}{c_\infty}\right)\right] + 2c_\infty^3 + \frac{c_\infty^4}{L}(1 - e^{-2L/c_\infty})\right\} \tag{21}$$

We can evaluate numerically $[\eta]_{a\text{-}KP}$ for $L/d \gtrsim 50$ from eq 2 and 3 with eq 19 and 21. This (OB) solution will be

Table I
Values of $\alpha_{jk}$ and $\beta_{jk}$ in Equation 24 for $d \leq 0.1$ and in Equation 35 for $d \leq 0.1c_\infty$

| $j$ | $\alpha_{j0}$ | $\alpha_{j1}$ | $\alpha_{j2}$ | $\beta_{j0}$ | $\beta_{j1}$ |
|---|---|---|---|---|---|
| 1 | 3.230 981 | −143.7458 | −1 906.263 | 2.463 404 | −1 422.067 |
| 2 | −22.461 49 | 1347.079 | 19 387.400 | −5.318 869 | 13 868.57 |
| 3 | 54.816 90 | −3235.401 | −49 357.06 | 15.417 44 | −34 447.63 |
| 4 | −32.919 52 | 2306.793 | 36 732.64 | −8.516 339 | 25 198.11 |

Table II
Values of $\alpha_{jk}$ and $\beta_{jk}$ in Equation 24 for $0.1 < d < 1.0$ and in Equation 35 for $0.1c_\infty < d < c_\infty$

| $j$ | $\alpha_{j0}$ | $\alpha_{j1}$ | $\alpha_{j2}$ | $\beta_{j0}$ | $\beta_{j1}$ |
|---|---|---|---|---|---|
| 1 | 6.407860 | −25.43785 | 23.33518 | 3.651 970 | −25.73698 |
| 2 | −115.0086 | 561.0286 | −462.8501 | −33.691 43 | 523.6108 |
| 3 | 318.0792 | −1625.451 | 1451.374 | 92.134 27 | −1508.112 |
| 4 | −144.5268 | 661.6760 | −1057.731 | −42.415 52 | 211.6622 |

Table III
Values of $b_{jk}$ in Equation 29

| $j$ | $b_{j0}$ | $b_{j1}$ | $b_{j2}$ |
|---|---|---|---|
| 1 | 5.948 14 | −4.906 78 | 2.563 81 |
| 2 | −22.770 5 | 14.663 1 | −7.248 94 |
| 3 | 42.520 0 | −25.874 1 | 11.415 8 |
| 4 | −25.837 2 | 15.268 1 | −4.324 30 |
| 5 | 7.480 88 | −4.225 95 | 0.298 512 |

referred to in the next section.

On the other hand, however, an expression for $[\eta]_{a\text{-KP}}$ may readily be obtained from that for $[\eta]_{KP}(L,d)$ as a function of $L$ and $d$ as follows,

$$[\eta]_{a\text{-KP}} = c_\infty{}^3[\eta]_{KP}(c_\infty{}^{-1}L, c_\infty{}^{-1}d) \tag{22}$$

Thus, we construct empirical interpolation formulas first for $[\eta]_{KP}$ ($c_\infty = 1$) and then for $[\eta]_{a\text{-KP}}$ from eq 22. For this purpose, it is convenient to make a slight modification of the previous expressions[4] for $[\eta]_{KP}$.

For $L \geq 2.278$, $[\eta]_{KP}$ may be expressed in the form,

$$[\eta]_{KP} = (\Phi_\infty L^{3/2}/M)(1 - \sum_{j=1}^{4} C_j L^{-j/2})^{-1} \qquad (L \geq 2.278) \tag{23}$$

with

$$C_j = \sum_{k=0}^{2} \alpha_{jk} d^k + \sum_{k=0}^{1} \beta_{jk} d^{2k} \ln d \qquad (j = 1\text{–}4) \tag{24}$$

where $\Phi_\infty = 2.870 \times 10^{23}$, and $\alpha_{jk}$ and $\beta_{jk}$ are constants independent of $L$ and $d$; their values, which are different for $d \leq 0.1$ and for $0.1 < d < 1.0$, are given in Tables I and II. The values of $\alpha_{jk}$ and $\beta_{jk}$ given in Table I for $d \leq 0.1$ are identical with the numerical coefficients in eq 38 of ref 4, while the values in Table II for $0.1 < d < 1.0$ are different from the numerical coefficients in eq 39 of ref 4.[10] We have redetermined these values to join smoothly eq 23 and a newly constructed empirical equation for $L < 2.278$ (which is given below) even for $d > 0.1$. We note that eq 23 with eq 24 is applicable for $L \geq 2.278$ when $d \leq 0.2$ and for $L^{1/2}/d \gtrsim 30$ when $0.2 < d < 1.0$, and the values of $[\eta]_{KP}$ calculated from them then agree with those from Table I of ref 4 to within 1.5%.

For $L < 2.278$, we write $[\eta]_{KP}$ in the form,

$$[\eta]_{KP} = [\eta]_{rod} f(L) \qquad (L < 2.278) \tag{25}$$

where $[\eta]_{rod}$ is the intrinsic viscosity of spheroid-cylinders, so that $f(L)$ is different from the function $f(L)$ in eq 40 of ref 4 but independent of $d$ as before (see below). For the spheroid-cylinder such that its total length is $L$ and the length of its intermediate cylinder part is $L - \epsilon d$, so that $\epsilon$ is the ratio of the principal diameters of the spheroid composed of its end parts, $[\eta]_{rod}$ may be expressed in the form,

$$[\eta]_{rod} = \frac{\pi N_A L^3}{24M} F_\eta(L/d,\epsilon) \tag{26}$$

with

$$F_\eta(p,\epsilon)^{-1} = \ln p + 2\ln 2 - 7/3 - 0.548250(\ln p)^{-1} - 11.1231p^{-1} \qquad \text{for } p \geq 100$$

$$F_\eta(p,\epsilon)^{-1} = 15/16\{\ln p + 2\ln 2 - 25/12 + b_0[\ln(1+p)]^{-1} + \sum_{j=1}^{5} b_j p^{-j/4}\} \qquad \text{for } \epsilon \leq p < 100 \tag{27}$$

where $b_j$ ($j = 0$–5) are functions of $\epsilon$ and are given by

$$b_0 = [\ln(1+\epsilon)][f_\eta(\epsilon)^{-1} - \ln\epsilon - 2\ln 2 + 25/12 - \sum_{j=1}^{5} b_j \epsilon^{-j/4}] \tag{28}$$

$$b_j = \sum_{k=0}^{2} b_{jk}\epsilon^k \qquad (j = 1\text{–}5) \tag{29}$$

$$f_\eta(\epsilon) = \frac{3}{2\epsilon^2}(\epsilon^2-1)^2\left\{\frac{-(4\epsilon^2-1)F + 2\epsilon^3 + \epsilon}{3\epsilon(3F + 2\epsilon^3 - 5\epsilon)[(2\epsilon^2+1)F - 3\epsilon]} + \frac{14}{3\epsilon(3F + 2\epsilon^3 - 5)} + \frac{2}{(\epsilon^2+1)(-3\epsilon F + \epsilon^2 + 2)} + \frac{\epsilon^2 - 1}{\epsilon(\epsilon^2+1)[(2\epsilon^2-1)F - \epsilon]}\right\} \qquad \text{for } \epsilon \neq 1$$

$$f_\eta(\epsilon) = 75/8 \qquad \text{for } \epsilon = 1 \tag{30}$$

with

$$F = (\epsilon^2-1)^{-1/2}\cosh^{-1}\epsilon \qquad \text{for } \epsilon > 1$$

$$F = (1-\epsilon^2)^{-1/2}\cos^{-1}\epsilon \qquad \text{for } \epsilon < 1 \tag{31}$$

The values of the numerical constants $b_{jk}$ in eq 29 are given in Table III. Equation 26 has been constructed to give the OB solution for rods with the preaveraged Oseen tensor[4,5] for $L/d \geq 100$ and to become the previous expression for spheroid-cylinders[6] for $L/d < 100$, and therefore the range of its application is limited to $0.6 \leq \epsilon \leq 1.3$. (For the validity of this connection, see ref 6.) Note that when $\epsilon = 1$, the spheroid-cylinder becomes the (prolate) spherocylinder, i.e., the cylinder with hemisphere caps at the ends.

From the numerical solutions for $[\eta]_{KP}$ for $L < 2.278$ and $d \leq 0.1$ (Table II of ref 4[11]), the function $f$ in eq 25 has

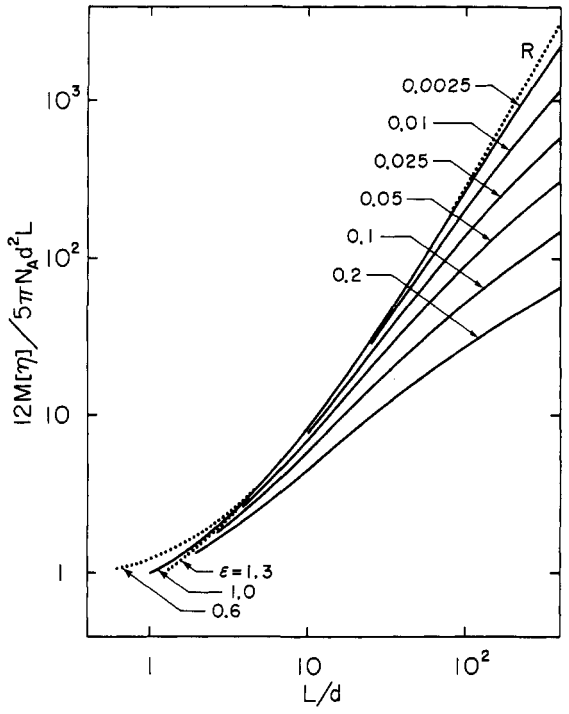


**Figure 1.** Double logarithmic plots of $12M[\eta]/5\pi N_A d^2 L$ against $L/d$. The full curves represent the values for the KP chain with $\epsilon = 1$, the numbers attached to the curves indicating the values of $d$. The dotted curves (R) represent the values for the spheroid-cylinders with the indicated values of $\epsilon$.

proved to be almost independent of $d$ and $\epsilon$ and may be approximated by

$$f(L) = 1 - \sum_{j=1}^{5} C_j L^j \tag{32}$$

where the numerical constants $C_j$ have been determined by the method of least squares to be

$$\begin{aligned} C_1 &= 0.321\,593 & C_2 &= 0.046\,638\,4 \\ C_3 &= -0.106\,466 & C_4 &= 0.037\,931\,7 \\ C_5 &= -0.003\,995\,76 \end{aligned} \tag{33}$$

Equation 25 with eq 32 predicts that $[\eta]_{KP}$ becomes $[\eta]_{rod}$ in the limit $L \to 0$ ($\lambda^{-1} \to \infty$), as required from the physical point of view. However, note that $L$ cannot become zero at finite constant $d$, since $L/d \geq \epsilon$ for the spheroid-cylinder. Although eq 25 with eq 32 has been constructed on the basis of the numerical solutions for $d \leq 0.1$, we assume that these equations are useful also for $d$ somewhat greater than 0.1. In order to examine the range of their validity, we consider the values of $[\eta]$ at $L = \epsilon d$. For $d \ll 1$ ($\lambda^{-1} \gg 1$), the KP chain with $L = \epsilon d$ may be regarded as the rigid spheroid of principal diameters $L$ and $d$, since then $f(\epsilon d) \simeq 1$. This is not unnatural. As $d$ is increased ($\lambda^{-1}$ is decreased), $f(\epsilon d)$ becomes appreciably smaller than unity. The KP chain with $L = \epsilon d$ may then be regarded as the deformable spheroid. However, we do not know the correct values of $[\eta]$ for the latter. For convenience, therefore, we limit the range of application of eq 25 with eq 32 to $d \leq 0.2$, in which range $[\eta]_{KP}$ does not appreciably differ from $[\eta]_{rod}$ at $L/d \simeq \epsilon$. Indeed, for $d \leq 0.2$, eq 23 and 25 are joined smoothly at $L = 2.278$.

Figure 1 shows double logarithmic plots of $12M[\eta]/5\pi N_A d^2 L$ against $L/d$. The full curves represent the values calculated from eq 23 and 25 for the KP chain with $\epsilon = 1$, the numbers attached to the curves indicating the values of $d$. The dotted curves (R) represent the values calculated from eq 26 for the spheroid-cylinders with $\epsilon = 0.6$, 1, and 1.3, which differ appreciably from one another only for $L/d \lesssim 5$.

Finally, it is straightforward to write expressions for $[\eta]_{a\text{-KP}}$ by the use of eq 22–33. The results are

$$[\eta]_{a\text{-KP}} = (c_\infty^{3/2}\Phi_\infty L^{3/2}/M) \times (1 - \sum_{j=1}^{4} c_\infty^{j/2} C_j L^{-j/2})^{-1} \quad \text{for } L \geq 2.278 c_\infty \tag{34}$$

with

$$C_j = \sum_{k=0}^{2} c_\infty^{-k} \alpha_{jk} d^k + \sum_{k=0}^{1} c_\infty^{-2k} \beta_{jk} d^{2k} \ln (c_\infty^{-1} d) \quad (j = 1\text{–}4) \tag{35}$$

and

$$[\eta]_{a\text{-KP}} = \frac{\pi N_A L^3}{24M} F_\eta(L/d,\epsilon) f(c_\infty^{-1} L) \quad L < 2.278 c_\infty \tag{36}$$

where the values of $\alpha_{jk}$ and $\beta_{jk}$ are given in Table I for $d \leq 0.1 c_\infty$ and in Table II for $0.1 c_\infty < d < c_\infty$, and $F_\eta$ and $f$ are given by eq 27–33. We note that eq 34 is valid for $L^{1/2}/d \gtrsim 30 c_\infty^{-1/2}$ when $d > 0.2 c_\infty$, eq 36 is valid for $d \leq 0.2 c_\infty$, and eq 34–36 reduce to the corresponding equations for the KP chain when $c_\infty = 1$ ($\kappa_0 = 0$).

## Numerical Solutions

It is known that the equilibrium average quantities such as $\langle R^2 \rangle$, $\langle S^2 \rangle$, and $\langle R^{-1} \rangle$ as functions of $L$ exhibit oscillations in the range of $L \lesssim 1.0$ for typical HW chains.[2,8] In part 2,[1] it was also seen that the sedimentation coefficient exhibits inflections in the same range. For HW chains having such oscillatory properties, it cannot be expected that we obtain accurate numerical solutions for $[\eta]$ from eq 2 and 3 with eq 7 and 16 by the method of Schlitt,[12] in which the integrals are evaluated by using $n$-point Gaussian quadratures ($n$ = 40–100), followed by extrapolation to $n = \infty$. The reason for this is that the variation in the mean reciprocal distance or the kernel is not sufficiently slow within every interval of the variable of integration unless $n$ is extremely large. Indeed, the extrapolated values of $[\eta]$ ($n \to \infty$) exhibit oscillations over the relatively wide range $10 \lesssim L \lesssim 60$. Of course, this is not a real reflection of the helical nature but a consequence of the above unpleasant situation at finite $n$; $[\eta]$ must be a monotonic function of $L$ in this range.

However, we have found that as $n$ is increased, the oscillation becomes less remarkable and occurs in a narrower range of $L \simeq 60$. Thus, we use the following maneuver to obtain accurate values of $[\eta]$. We evaluate both $[\eta]$ and $[\eta]_{a\text{-KP}}$ at $n = 80$ (from eq 2 and 3 with eq 7, 16, 19, and 21) and adopt the ratio $\Gamma_\eta = [\eta]/[\eta]_{a\text{-KP}}$ of these solutions as the correct one. Indeed, this procedure makes the oscillation almost disappear and gives the values of $\Gamma_\eta$ which agree with its extrapolated values ($n \to \infty$) to within 1% over the range in which no oscillation occurs. The values of $\Gamma_\eta$ thus obtained are represented by the full curves in Figure 2 for the two cases of $\mu = 0.2$ and $\nu = 2$ (weak helical nature) and of $\mu = 0.2$ and $\nu = 8$ (strong helical nature), both with $d = 0.01$. The open circles represent the values obtained from the extrapolated values of $[\eta]$ with the values of $[\eta]_{a\text{-KP}}$ calculated from eq 34. For the case of weak helical nature, there is good agreement between the full curve and the open circles without oscillations. On the other hand, for the case of strong helical nature, the open circles oscillate in the range $10 \lesssim L \lesssim 60$, while the full curve is almost smooth. (The small oscillation in the latter at $L \simeq 40$ will be smeared out in the construction of an

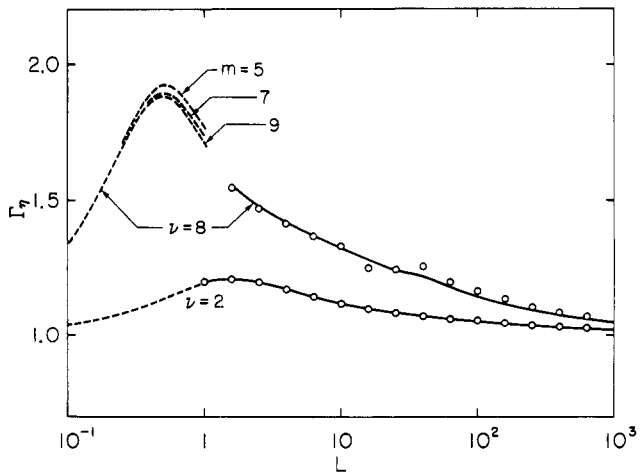


**Figure 2.** $\Gamma_\eta$ plotted against the logarithm of $L$ for the two cases of $\mu = 0.2$ and $\nu = 2$ and of $\mu = 0.2$ and $\nu = 8$, both with $d = 0.01$. The full curves represent the values obtained by the method of Schlitt with 80-point Gaussian quadratures, and the open circles represent the corresponding extrapolated values. The broken curves represent the values obtained from the Legendre polynomial expansions truncated at $m = 9$ for the case of $\mu = 0.2$ and $\nu = 2$ and at the indicated $m$ for the case of $\mu = 0.2$ and $\nu = 8$.

interpolation formula.) We note that all numerical work has been done with the use of a FACOM M-200 digital computer at this University.

For $L/d \lesssim 50$, the accuracy of the numerical solution of the integral eq 3 becomes very bad for both HW and KP chains. In other words, this inaccuracy is not peculiar to HW chains. We must therefore adopt another maneuver in this range. (Of course, we are considering the range of $L/d \gtrsim 10$ in which the OB solution is valid.)

Now, we expand the solution $\psi$ and the known part $g$ in terms of the Legendre polynomials $P_j$,

$$\psi(x,y) = \sum_{j=0}^{\infty} \lambda_j^{-1} \psi_j(y) P_j(x) \tag{37}$$

$$g(x,y) = \sum_{j=0}^{\infty} \lambda_j^{-1} g_j(y) P_j(x) \tag{38}$$

where

$$\lambda_j = \int_{-1}^{1} [P_j(x)]^2 \, dx \tag{39}$$

$$\psi_j(y) = \int_{-1}^{1} \psi(x,y) P_j(x) \, dx \tag{40}$$

and a similar equation holds for $g_j(y)$. Substitution of eq 37 and 38 into eq 3 and integration over $x$ of both sides multiplied by $P_j(x)$ leads to

$$\sum_{k=0}^{\infty} \lambda_k^{-1} K_{jk} \psi_k(y) = g_j(y) \tag{41}$$

with

$$K_{jk} = \int_{-1}^{1} \int_{-1}^{1} K(x,y) P_j(x) P_k(y) \, dx \, dy \tag{42}$$

Substitution of the solution of eq 41 into eq 37 leads to

$$\psi(x,y) = \sum_{j=0}^{\infty} \sum_{k=0}^{\infty} A_{jk} g_k(y) P_j(x) \tag{43}$$

where $A_{jk}$ is the $jk$ element of the inverse of the infinite matrix $(K_{jk})$. Thus, we have, from eq 2 and 43,

$$[\eta] = (N_A L/M) \sum_{j=0}^{\infty} \sum_{k=0}^{\infty} A_{jk} g_{jk} \tag{44}$$

with

$$g_{jk} = \int_{-1}^{1} \int_{-1}^{1} g(x,y) P_j(x) P_k(y) \, dx \, dy \tag{45}$$

(Note that only $g_{11}$ is nonzero in the case of rods.[4]) As was done by Taki,[13] we then truncate the Legendre polynomial expansions to approximate eq 44 by

$$[\eta] = (N_A L/M) \sum_{j=0}^{m} \sum_{k=0}^{m} A_{jk}^{(m)} g_{jk} \tag{46}$$

where $A_{jk}^{(m)}$ is the $jk$ element of the inverse of the $(m + 1) \times (m + 1)$ matrix $(K_{jk})$ $(j, k = 0, 1, ..., m)$. We have found that if we use the values of $[\eta]$ and $[\eta]_{a\text{-KP}}$ calculated from eq 46 for various values of $m$, the convergence of the ratio $\Gamma_\eta$ itself is rather good for small $L/d$, especially for cases of weak helical nature. The values of $\Gamma_\eta$ thus evaluated are also represented by the broken curves in Figure 2 for the two cases. In the case of $\nu = 2$ (and $\mu = 0.2$), the convergence is very good, and only the $m = 9$ values are shown.

Thus, in order to construct an empirical interpolation formula for $\Gamma_\eta$ in the next section, we adopt its (OB) values obtained by the method of Schlitt with $n = 80$ (for relatively large $L$) and by the Legendre polynomial expansion truncated at $m = 9$ (for small $L$).

## Empirical Equations

We construct an interpolation formula for the factor $\Gamma_\eta$ as a function of $L$, $d$, $\kappa_0$, and $\tau_0$ in the equation,

$$[\eta] = [\eta]_{a\text{-KP}} \Gamma_\eta(L,d;\kappa_0,\tau_0) \tag{47}$$

where $[\eta]_{a\text{-KP}}$ is given by eq 34 or 36. The motivation is therefore similar to that in the case of the sedimentation coefficient.[1] A good approximation to $\Gamma_\eta$ has been found to be of the form,

$$\Gamma_\eta = 1 + (A_1 L^{-1/2} + A_2 L^{-1})[1 - (1 + \xi L)e^{-\xi L}] + A_3 L^{-3/2}\{1 - [1 + \xi L + \tfrac{1}{2}(\xi L)^2]e^{-\xi L}\} + A_4 L e^{-\xi L} \tag{48}$$

with

$$A_l = \sum_{j=0}^{3} \sum_{k=0}^{3} \left( \sum_{m=0}^{2} a_{jk}^{lm} d^m + a_{jk}^{l3} \ln d \right) \nu^k \cos(j\pi\mu) \qquad (l = 1\text{–}4) \tag{49}$$

where $\xi$ is a constant weakly dependent on $\mu$ and $\nu$, and $a_{jk}^{lm}$ are constants independent of $L$, $d$, $\kappa_0$, and $\tau_0$. We note that the second and third terms on the right-hand side of eq 48 have been inferred to give the analytically predicted asymptotic forms,

$$\lim_{L \to 0} \Gamma_\eta = 1 + (\text{constant})L \tag{50}$$

$$\lim_{L \to \infty} \Gamma_\eta = 1 + (\text{constant})L^{-1/2} \tag{51}$$

and the fourth term has been added to give good approximations. Further, note that $A_l$ is of the same form as that in the sedimentation coefficient.[1]

The constants $\xi$ and $a_{jk}^{lm}$ have been determined by the method of least squares on the basis of the values of $\Gamma_\eta$ calculated following the procedure of the preceding section for various values of $L$ ranging from 0.04 to 1000, and of $d$ ranging from 0.0025 to 0.1 (see ref 1). We have again chosen the values of $\kappa_0$ and $\tau_0$ indicated by the filled points in the $(\kappa_0,\tau_0)$ plane of Figure 3 of part 2.[1] Thus, a best form of $\xi$ has been found to be

$$\xi = 0.3 + 0.4\nu \tag{52}$$

The results for $a_{jk}^{lm}$ are given in Tables IV and V. The

Table IV
Values of $a_{jk}^{1m}$ and $a_{jk}^{2m}$ in Equation 49

| $j$ | $k$ | $a_{jk}^{10}$ | $a_{jk}^{11}$ | $a_{jk}^{12}$ | $a_{jk}^{13}$ | $a_{jk}^{20}$ | $a_{jk}^{21}$ | $a_{jk}^{22}$ | $a_{jk}^{23}$ |
|---|---|---|---|---|---|---|---|---|---|
| 0 | 0 | −2.0560 | −3.3009 | −9.2712(1) | −6.8292(−2) | 1.5062(1) | −2.7067(2) | 7.1712(2) | 2.2787 |
| 0 | 1 | 2.0338 | 5.7923 | 2.9984(1) | 7.6822(−2) | −1.0938(1) | 1.7162(2) | 1.7702(1) | −1.6192 |
| 0 | 2 | −5.3442(−1)[a] | −7.2935(−1) | −4.6034 | −2.8443(−2) | 2.6271 | −3.6987(1) | −1.0020(2) | 3.9703(−1) |
| 0 | 3 | 3.9862(−2) | −7.1564(−2) | 6.0721(−1) | 2.8259(−3) | −1.9957(−1) | 2.7950 | 1.1020(1) | −3.0949(−2) |
| 1 | 0 | 1.5577 | 2.5311(1) | −3.6036 | −9.0219(−2) | −1.3200(1) | 2.5285(2) | 5.2500(2) | −2.1955 |
| 1 | 1 | −1.7624 | −1.9228(1) | 3.0894(1) | 1.3367(−2) | 1.1275(1) | −1.8668(2) | −1.0216(3) | 1.8375 |
| 1 | 2 | 7.2816(−1) | 3.5121 | −8.2356 | 2.9879(−2) | −3.3222 | 4.3384(1) | 3.7191(2) | −5.1895(−1) |
| 1 | 3 | −6.3119(−2) | −1.5462(−2) | −2.2994(−1) | −4.1216(−3) | 2.8525(−1) | −3.6840 | −3.0926(1) | 4.4758(−2) |
| 2 | 0 | −1.2666 | −1.5478(1) | 4.2503(1) | 2.7719(−2) | 7.8342 | −1.1931(2) | −6.9702(2) | 1.2287 |
| 2 | 1 | 1.2587 | 1.0763(1) | −4.2160(1) | 1.0918(−2) | −6.7202 | 9.1345(1) | 8.1661(2) | −1.0491 |
| 2 | 2 | −3.8031(−1) | −1.4646 | 8.4172 | −1.6815(−2) | 1.8848 | −2.2973(1) | −2.4715(2) | 2.9708(−1) |
| 2 | 3 | 3.1480(−2) | −3.1514(−2) | −1.3980(−1) | 2.2289(−3) | −1.5839(−1) | 1.9979 | 1.9596(1) | −2.5388(−2) |
| 3 | 0 | 8.0993(−1) | 8.0567 | −2.3310(1) | 9.1452(−3) | −2.8403 | 3.3882(1) | 3.9886(2) | −4.1058(−1) |
| 3 | 1 | −8.2936(−1) | −5.7999 | 1.8462(1) | −2.5547(−2) | 2.6533 | −2.7952(1) | −3.9750(2) | 3.7724(−1) |
| 3 | 2 | 2.5352(−1) | 9.7040(−1) | −3.1344 | 1.2912(−2) | −7.9375(−1) | 7.5183 | 1.1243(2) | −1.1282(−1) |
| 3 | 3 | −1.9288(−2) | −3.2201(−3) | −4.6997(−2) | −1.2939(−3) | 6.8030(−2) | −7.4523(−1) | −8.4249 | 1.0024(−2) |

[a] $a(n)$ means $a \times 10^n$.

Table V
Values of $a_{jk}^{3m}$ and $a_{jk}^{4m}$ in Equation 49

| $j$ | $k$ | $a_{jk}^{30}$ | $a_{jk}^{31}$ | $a_{jk}^{32}$ | $a_{jk}^{33}$ | $a_{jk}^{40}$ | $a_{jk}^{41}$ | $a_{jk}^{42}$ | $a_{jk}^{43}$ |
|---|---|---|---|---|---|---|---|---|---|
| 0 | 0 | −1.6187(1)[a] | 2.6005(2) | 2.8360(2) | −2.6072 | −1.4233(1) | −3.2493(2) | −1.4450(3) | −2.7437 |
| 0 | 1 | 1.0524(1) | −1.4953(2) | −9.7455(2) | 1.6915 | 1.1871(1) | 3.1928(2) | 8.3429(2) | 2.3242 |
| 0 | 2 | −2.3777 | 2.8669(1) | 3.6369(2) | −3.9136(−1) | −2.9705 | −8.4549(1) | −1.4034(2) | −6.1080(−1) |
| 0 | 3 | 1.7933(−1) | −2.0245 | −3.1991(1) | 3.0082(−2) | 2.1514(−1) | 5.8955 | 7.5902 | 4.6005(−2) |
| 1 | 0 | 1.1353(1) | −1.6515(2) | −2.7938(3) | 2.2422 | 2.0308(1) | 6.5344(2) | 1.3019(3) | 3.7915 |
| 1 | 1 | −9.4901 | 1.1250(2) | 2.9900(3) | −1.8315 | −1.9245(1) | −5.9239(2) | −6.7112(2) | −3.5060 |
| 1 | 2 | 2.6477 | −2.2930(1) | −8.9281(2) | 4.8604(−1) | 5.5369 | 1.5126(2) | 8.3901(1) | 9.8570(−1) |
| 1 | 3 | −2.3297(−1) | 1.9932 | 7.1732(1) | −4.1733(−2) | −4.0796(−1) | −1.0125(1) | −6.8941 | −7.8071(−2) |
| 2 | 0 | −5.9585 | 5.5567(1) | 2.1353(3) | −1.1128 | −1.1608(1) | −3.7955(2) | −8.1729(2) | −2.3971 |
| 2 | 1 | 4.9895 | −3.8531(1) | −2.0283(3) | 9.2137(−1) | 1.0568(1) | 3.4593(2) | 4.6594(2) | 2.1656 |
| 2 | 2 | −1.4279 | 8.9932 | 5.5792(2) | −2.5949(−1) | −2.8796 | −8.9167(1) | −6.6441(1) | −5.8954(−1) |
| 2 | 3 | 1.2666(−1) | −9.0050(−1) | −4.3352(1) | 2.2754(−2) | 2.1600(−1) | 6.2056 | 3.0418 | 4.5547(−2) |
| 3 | 0 | 1.8460 | −1.0644(1) | −9.7087(2) | 3.4777(−1) | 5.4160 | 1.2851(2) | 2.3745(2) | 9.0560(−1) |
| 3 | 1 | −1.6976 | 8.4217 | 8.8667(2) | −3.0710(−1) | −4.9972 | −1.1412(2) | −1.4433(2) | −8.3608(−1) |
| 3 | 2 | 5.2276(−1) | −2.2320 | −2.3998(2) | 9.0803(−2) | 1.3555 | 2.8238(1) | 2.6879(1) | 2.3158(−1) |
| 3 | 3 | −4.9228(−2) | 3.1322(−1) | 1.8336(1) | −8.4882(−3) | −9.6194(−2) | −1.7567 | −2.8322 | −1.8132(−2) |

[a] $a(n)$ means $a \times 10^n$.

range of application of eq 47 with eq 48, 49, and 52 is limited to the shaded domain in the $(\kappa_0,\tau_0)$ plane of Figure 3 of part 2, to $0.0025 \leq d \leq 0.1$ for $c_\infty \geq 0.2$, and to $0.0025 \leq d \leq 0.075$ for $c_\infty < 0.2$. The ranges of application of eq 34 and 36 for $[\eta]_{a\text{-KP}}$ also apply to eq 47. In the range of its application, the error in the value of $\Gamma_\eta$ calculated from eq 47 does not exceed 1.5% except for $\mu < 0.1$ and $\nu > 3$ and for $0.1 \leq \mu < 0.3$ and $\nu > 4$, in which domains the possible maximum error is 4% for $L \lesssim 1$.

## Numerical Results

In this section, we examine the behavior of $[\eta]$ of HW chains on the basis of the values calculated from eq 47 with eq 48. For convenience, we consider only the case of $\epsilon = 1$. In all cases, the dependence on $\epsilon$ is remarkable only for $L/d \lesssim 5$ as in the case of spheroid-cylinders or rods (see Figure 1).

Figure 3 shows double logarithmic plots of $M[\eta]/\Phi_\infty L$ against $L$. The full and broken curves represent the values for a typical HW chain with $\mu = 0.2$, $\nu = 5$, and $d = 0.01$ and for the associated KP chain, respectively. In the figure, the values calculated from eq 26 for the rod and from eq 60 with eq 76 and 78 of part 1[5] for the corresponding characteristic helix are also represented by the dotted (R) and chain (H) curves, respectively. This figure corresponds to Figure 2 of part 2,[1] in which the case of $\nu = 8$ (instead of $\nu = 5$) is shown. It is known that the mean-square radius of the HW chain in general is greater than that of the associated KP chain, especially at $L \simeq$

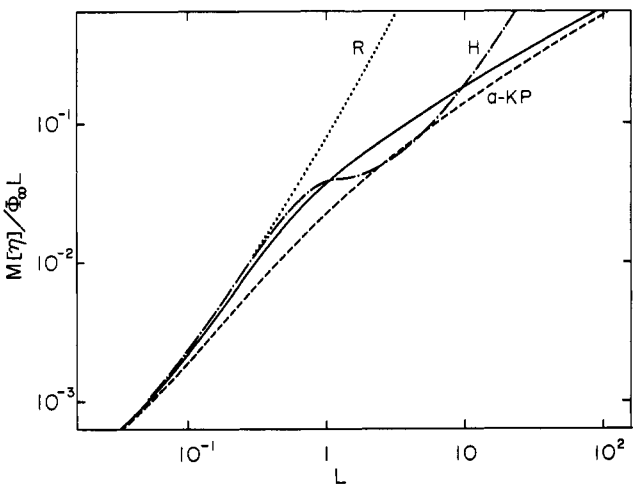


**Figure 3.** Double logarithmic plots of $M[\eta]/\Phi_\infty L$ against $L$. The full curve represents the values for the HW chain with $\mu = 0.2$, $\nu = 5$, and $d = 0.01$, and the broken curve a-KP, chain curve H, and dotted curve R represent the values for the associated KP chain, corresponding characteristic helix, and rod, respectively.

1. As a result, the HW chain has larger intrinsic viscosities $[\eta]$ and smaller sedimentation coefficients $s$ than does the associated KP chain. The difference between the two chains is more remarkable in $[\eta]$ than in $s$.

Figure 4 shows double logarithmic plots of $12M[\eta]/5\pi N_A d^2 L$ against $L/d$ for the two cases of $\nu = 2$ (weak

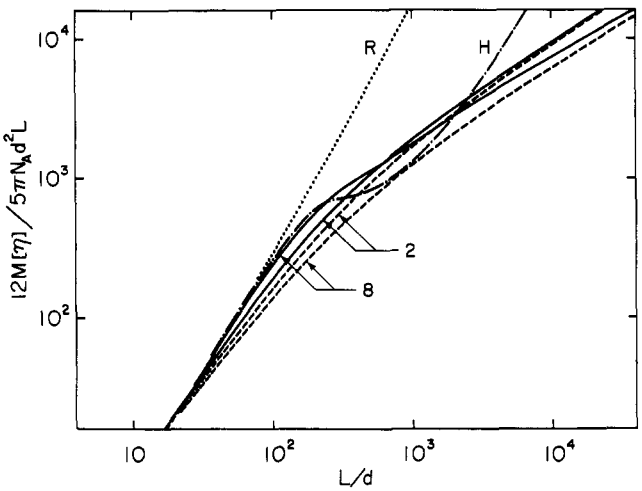


**Figure 4.** Double logarithmic plots of $12M[\eta]/5\pi N_A d^2 L$ against $L/d$ for the two cases of $\nu = 2$ and 8 when $\mu = 0.2$ and $\nu d = 0.02$. The full and broken curves represent the values for the HW chains and the corresponding associated KP chains, respectively, the numbers attached to the curves indicating the values of $\nu$. The chain curve H and dotted curve R represent the values for the corresponding characteristic helix and rod, respectively.

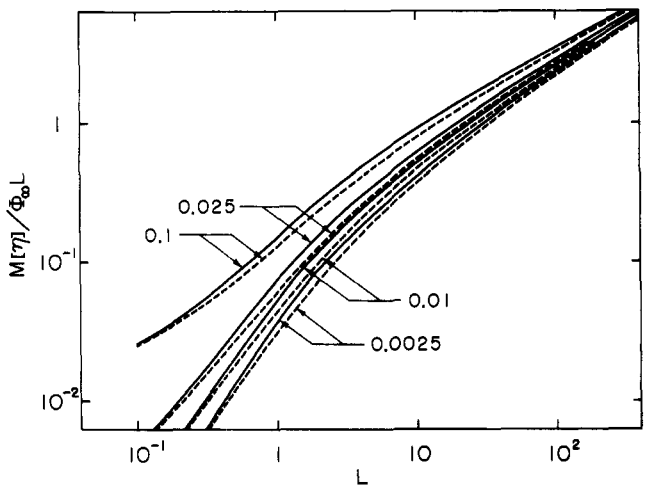


**Figure 5.** Double logarithmic plots of $M[\eta]/\Phi_\infty L$ against $L$ for $\mu = 0.2$ and $\nu = 2$. The full and broken curves represent the values for the HW and associated KP chains, respectively, the numbers attached to the curves indicating the values of $d$.

helical nature) and $\nu = 8$ (strong helical nature) when $\mu = 0.2$ and $\nu d = 0.02$. The full and broken curves represent the values for the HW chains and the associated KP chains, respectively, the numbers attached to the curves indicating the values of $\nu$. For comparison, the values for the corresponding characteristic helix and rod are also represented by the chain (H) and dotted (R) curves, respectively. Note that the characteristic helices corresponding to the HW chains with constant $\mu$ and $\nu d$ have the same ratio $M[\eta]/d^2L$ as a function of $L/d$.[5] This figure corresponds to Figure 4 of part 2. Thus, in this case, the helical nature of the chain with larger $\nu$ (larger $\lambda^{-1}$) is stronger, the unreduced $\kappa_0$, $\tau_0$, and $d$ being regarded as fixed. Indeed, the full curve for large $\nu$ (and small $d$) is close to the chain curve for the characteristic helix in the range of small $L/d$ and has an inflection point.

Figures 5 and 6 show double logarithmic plots of $M[\eta]/\Phi_\infty L$ against $L$ for the cases of $\mu = 0.2$ and $\nu = 2$ and of $\mu = 0.2$ and $\nu = 8$, respectively. The full and broken curves represent the values for the HW and associated KP chains, respectively, the numbers attached to the curves indicating the values of $d$. These figures correspond to

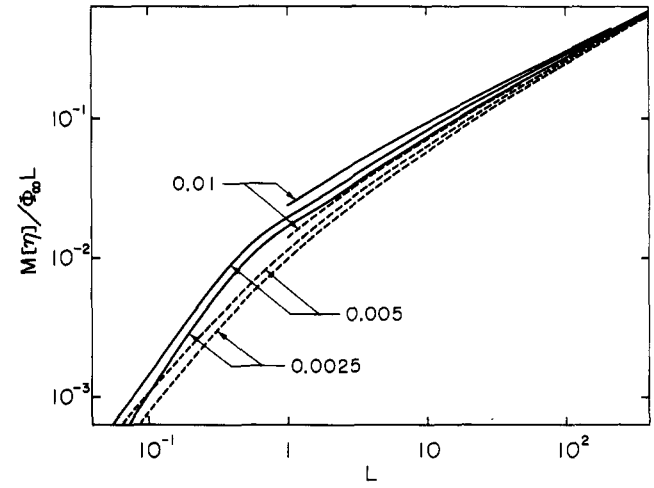


**Figure 6.** Double logarithmic plots of $M[\eta]/\Phi_\infty L$ against $L$ for $\mu = 0.2$ and $\nu = 8$; see legend to Figure 5.

Figures 5 and 6 of part 2, respectively. As $d$ is decreased, the slope of the plot increases in the case of $[\eta]$, while it decreases in the case of $s$. Further, we note that $[\eta]$ is proportional to $c_\infty^{3/2}$, as seen from eq 34 and 47, so that $[\eta]$ decreases for large $L$ as the helical nature is increased. (Recall that $c_\infty$ is smaller for the chain of stronger helical nature.) The situation is again opposite to the case of $s$. These relations are readily seen in Figures 5 and 6 of part 2 and the present paper.

## Analysis of Experimental Data

In this paper, we make an analysis of experimental data for the intrinsic viscosity $[\eta]$, sedimentation coefficient $s$, and mean-square radius of gyration $\langle S^2 \rangle$ as functions of the molecular weight $M$, taking as examples poly(phthaloyl-*trans*-2,5-dimethylpiperazine), poly(terephthaloyl-*trans*-2,5-dimethylpiperazine), cellulose acetate, and amylose. In this section, for convenience, we designate the reduced intrinsic viscosity and reduced mean-square radius of gyration by $[\tilde{\eta}]$ and $\langle \tilde{S}^2 \rangle$ to distinguish them from the unreduced $[\eta]$ and $\langle S^2 \rangle$, respectively, and $[\tilde{\eta}]$, $\langle \tilde{S}^2 \rangle$, $L$, $d$, $\kappa_0^{-1}$, and $\tau_0^{-1}$ are measured in units of $\lambda^{-1}$, all other quantities being unreduced unless specified otherwise.

We consider double logarithmic plots of $[\eta]$ (in dL/g) and $s$ (in Svedbergs) against $M$ by the use of the equations,

$$\log [\eta] = \log (M[\tilde{\eta}]/\Phi_\infty L) - \log (\lambda^2 M_L) - 2.542 \quad (53)$$

$$\log s = \log \tilde{s} + \log M_L + \log [(1 - \bar{v}\rho_0)/\eta_0] - 3.754 \quad (54)$$

with

$$\log M = \log L + \log (M_L/\lambda) \quad (55)$$

where $M_L$ is the shift factor as defined as the molecular weight per unit (unreduced) contour length of the chain, $[\tilde{\eta}]$ is given by eq 47 with $\Phi_\infty = 2.870 \times 10^{23}$, and $\tilde{s}$ is given by eq 28 of part 2[1] with $\bar{v}$ the partial specific volume of the polymer, $\rho_0$ the mass density of the solvent, and $\eta_0$ the viscosity coefficient (in Poises) of the latter, $\lambda^{-1}$ and $M_L$ being expressed in Å and Å$^{-1}$, respectively. Note that $M[\tilde{\eta}]/\Phi_\infty L$ and $\tilde{s}$ are functions of $L$, $d$, $\kappa_0$, and $\tau_0$. Thus, the quantities $M_L/\lambda$ and $\lambda^2 M_L$ (and therefore $\lambda^{-1}$ and $M_L$) may be determined from a best fit of double logarithmic plots of the theoretical $M[\tilde{\eta}]/\Phi_\infty L$ (for proper $\kappa_0$, $\tau_0$, and $d$, and also $\epsilon$ if necessary) against $L$ to double logarithmic plots of observed $[\eta]$ against $M$, and the quantities $M_L/\lambda$ and $M_L$ (and therefore $\lambda^{-1}$ and $M_L$) may be determined from a best fit of double logarithmic plots of the theoretical $\tilde{s}$ against $L$ to double logarithmic plots of observed $s$ against $M$.

Table VI
Values of the Model Parameters of Various Stiff Chains

| polymer | solvent | model | $\kappa_0$ | $\tau_0$ | $\rho$, Å | $h$, Å | $\lambda^{-1}$, Å | $M_L$, Å$^{-1}$ | $d$, Å |
|---|---|---|---|---|---|---|---|---|---|
| PPDP[a] | NMP (25 °C) | HW | 1.96 | 0.4 | 59 | 75 | 120 | 38 | 3.6 |
| PTDP[b] | TFE (25 °C) | KP | 0 | | 0 | | 110 | 37 | 6.6 |
| CAc[c] | TFE (20 °C) | HW | 1.96 | 0.4 | 180 | 230 | 370 | 54 | 5.2 |
| amylose[d] | $Me_2SO$ (25 °C) | HW | 4.90 | 1.0 | 120 | 160 | 630 | 79 | 12.6 |

[a] See ref 17. [b] See ref 18. [c] See ref 25. [d] See ref 30.

For rods or those with small flexibility, it is more convenient to use, instead of eq 53, the equation,

$$\log [\eta] = \log (12M[\bar{\eta}]/5\pi N_A d^2 L) + \log (d^2/\lambda^2 M_L) - 2.103 \quad (56)$$

with

$$\log M = \log (L/d) + \log (M_L d/\lambda) \quad (57)$$

In this case, the quantities $M_L d/\lambda$ and $d^2/\lambda^2 M_L$ (and therefore $d/\lambda$, i.e., the unreduced $d$, and $M_L$) may be determined from a best fit of double logarithmic plots of the theoretical $12M[\bar{\eta}]/5\pi N_A d^2 L$ (for proper $\kappa_0$, $\tau_0$, $d$, and $\epsilon$) against $L$ to double logarithmic plots of $[\eta]$ against $M$.

As for the mean-square radius of gyration, in this paper, we consider, instead of $\langle S^2 \rangle$ itself, the ratio of $\langle S^2 \rangle$ to its coil limiting value $\langle S^2 \rangle_{(C)}$,

$$\langle S^2 \rangle_{(C)} = [\lim_{M \to \infty} (\langle S^2 \rangle / M)] M \equiv (\langle S^2 \rangle / M)_\infty M \quad (58)$$

The reason for this is that we retain the above theoretical value of $\Phi_\infty$[14] as before[4] despite the fact that there is sometimes disagreement between its theoretical and observed values even with corrections for the polydispersity. We then have

$$\log (\langle S^2 \rangle / \langle S^2 \rangle_{(C)}) = \log (6\langle \bar{S}^2 \rangle / c_\infty L) \quad (59)$$

with eq 55. Note that the ratios $\langle S^2 \rangle / \langle S^2 \rangle_{(C)}$ and $6\langle \bar{S}^2 \rangle / c_\infty L$ become unity in the limit $M$ and $L \to \infty$. Thus, we determine $M_L/\lambda$ from a best fit of double logarithmic plots of the theoretical $6\langle \bar{S}^2 \rangle / c_\infty L$ (for proper $\kappa_0$ and $\tau_0$) against $L$ to double logarithmic plots of observed $\langle S^2 \rangle / \langle S^2 \rangle_{(C)}$ against $M$.

**Poly(phthaloyl-*trans*-2,5-dimethylpiperazine).** Motowoka et al.[17] measured $[\eta]$, $s$, and $\langle S^2 \rangle$ on fractions of poly(phthaloyl-*trans*-2,5-dimethylpiperazine) (PPDP) in various solvents. We take here as an example the data in *N*-methyl-2-pyrrolidone (NMP) at 25 °C. In this case, they have obtained $\lambda^{-1}$ = 66 Å, $M_L$ = 33 Å$^{-1}$, and $d$ = 7.4 Å, assuming the KP chain but using a method different from ours above.

Now, double logarithmic plots of $[\eta]$ and $s$ against $M$ with their data are shown by the open circles in Figure 7, where $M$ is the weight-average molecular weight. The broken curves represent the best fit theoretical values calculated as the KP chain from eq 23, 25, 53, and 54 and eq 25 of part 2 (with $c_\infty$ = 1) with $d$ = 0.12, log $(M_L/\lambda)$ = 3.34, and log $(\lambda^2 M_L)$ = −1.98. From these, we obtain $\lambda^{-1}$ = 59 Å, $M_L$ = 37 Å$^{-1}$, and $d$ = 7.1 Å. The full curves represent the best fit theoretical values calculated as the HW chain from eq 47, 53, and 54 and eq 28 of part 2 with $\kappa_0$ = 1.96, $\tau_0$ = 0.4 ($\mu$ = 0.2, $\nu$ = 2.0), $d$ = 0.03, log $(M_L/\lambda)$ = 3.66, and log $(\lambda^2 M_L)$ = −2.58. We then obtain $\lambda^{-1}$ = 120 Å, $M_L$ = 38 Å$^{-1}$, and $d$ = 3.6 Å. It is important to note here that although $\lambda^{-1}$ is equal to the Kuhn segment length and is just twice the persistence length in the case of the KP chain, this relation does not hold for the HW chain with $\kappa_0 \neq 0$.[3] From Figure 7, it is seen that the slopes of the plots may be somewhat better explained by the HW chain than by the KP chain. Thus, the values of the model parameters of PPDP as the HW chain are listed in Table VI, where the values of the radius $\rho$ and pitch $h$ of the characteristic helix[3] are also given. The observed $\langle S^2 \rangle / M$ is almost independent of $M$, and therefore we cannot determine $M_L/\lambda$ from $\langle S^2 \rangle / \langle S^2 \rangle_{(C)}$.

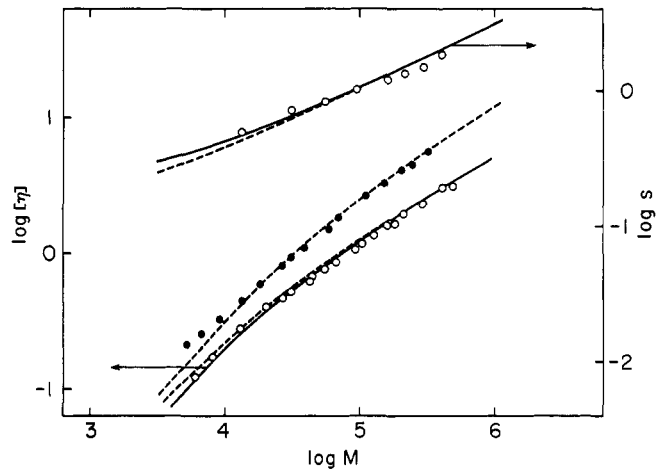


**Figure 7.** Analysis of the data for $[\eta]$ and $s$ for poly(phthaloyl-*trans*-2,5-dimethylpiperazine) in *N*-methyl-2-pyrrolidone at 25 °C (open circles)[17] and for poly(terephthaloyl-*trans*-2,5-dimethylpiperazine) in trifluoroethanol at 25 °C (filled circles)[18] according to eq 53 and 54 with eq 55. The full and broken curves represent the best fit theoretical values as the HW and KP chains, respectively.

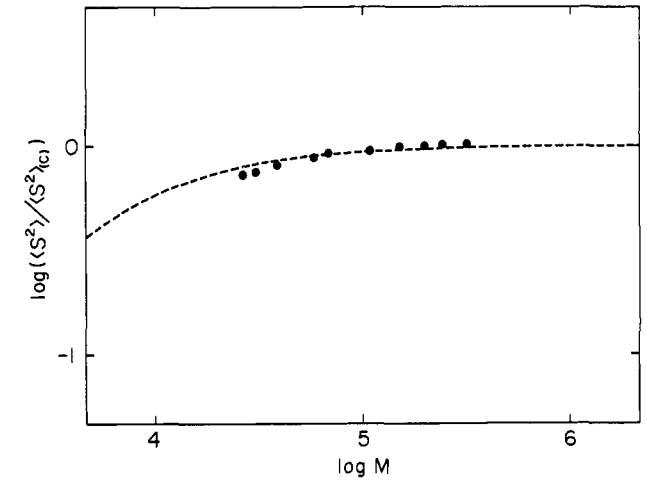


**Figure 8.** Analysis of the data for $\langle S^2 \rangle$ for poly(terephthaloyl-*trans*-2,5-dimethylpiperazine) in trifluoroethanol at 25 °C[18] according to eq 59 with eq 55. The broken curve represents the theoretical values as the KP chain.

**Poly(terephthaloyl-*trans*-2,5-dimethylpiperazine).** For comparison, the viscosity data obtained by Motowoka et al.[18] for poly(terephthaloyl-*trans*-2,5-dimethylpiperazine) (PTDP) in trifluoroethanol (TFE) at 25 °C are shown by the filled circles in Figure 7. (Note that $s$ has not been measured for this polymer.) The corresponding broken curve represents the best fit theoretical values as the KP chain with $d$ = 0.06, log $(M_L/\lambda)$ = 3.62, and log $(\lambda^2 M_L)$ = −2.54. We then obtain the values of the model

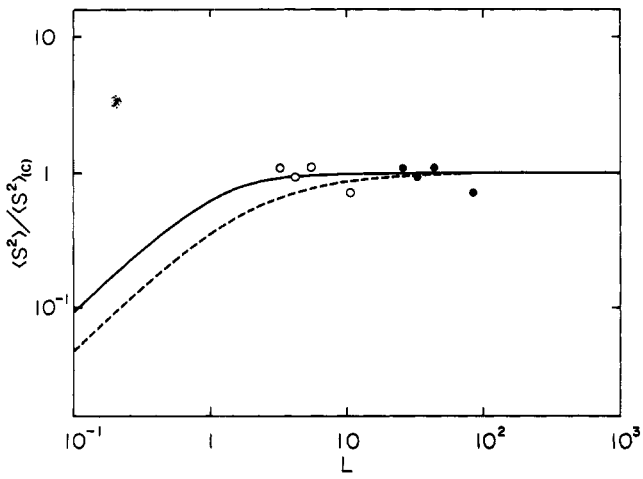


**Figure 9.** Double logarithmic plots of $\langle S^2\rangle/\langle S^2\rangle_{(C)}$ against $L$ for cellulose acetate in trifluoroethanol at 20 °C[25] with the displacements log $(M_L/\lambda)$ = 4.3 and 3.4 for the open and filled circles, respectively. The full and broken curves represent the theoretical values as the HW and KP chains corresponding to the open and filled circles, respectively.

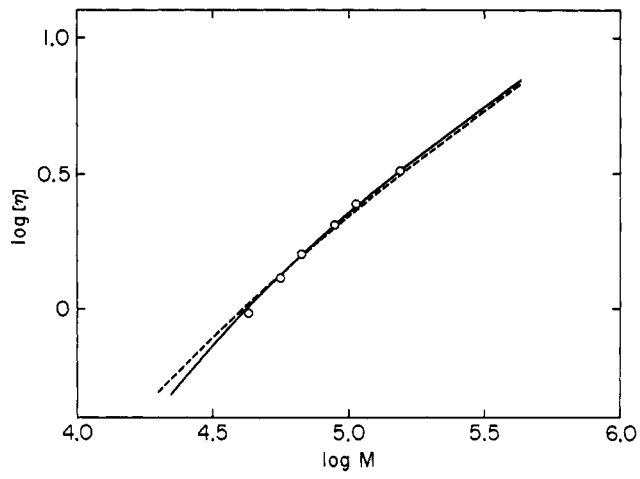


**Figure 10.** Analysis of the data for $[\eta]$ for cellulose acetate in trifluoroethanol at 20 °C[25] according to eq 53 with eq 55. The full and broken curves represent the best fit theoretical values as the HW and KP chains, respectively.

parameters given in Table VI. Figure 8 shows double logarithmic plots of $\langle S^2\rangle/\langle S^2\rangle_{(C)}$ against $M$ for the same system with $(\langle S^2\rangle/M)_\infty$ = 0.594 Å$^2$, and the broken curve represents the theoretical values calculated as the KP chain from eq 15 and 59 ($c_\infty$ = 1) with the same $M_L/\lambda$ as above. In the case of $[\eta]$, the agreement between theory and experiment is not good for $M \lesssim 10^4$. Note that in this range, the end effect cannot be remarkable according to the present theory, since the lowest measured molecular weight corresponds to $L/d \simeq 20$ if we adopt the above values of $M_L$ and $d$. Thus, we have reanalyzed the data assuming the HW chain and found that the agreement between theory and experiment is much improved with $\kappa_0$ = 1.96, $\tau_0$ = 0.4, $\epsilon$ = 1, $\lambda^{-1}$ = 310 Å, $M_L$ = 64 Å$^{-1}$, and $d$ = 31 Å. However, these values of $M_L$ and $d$ are unreasonably large, considering the local structure of the PTDP chain. The assumption of the HW chain for PTDP should therefore be rejected. Thus, the above disagreement between theory and experiment at small $M$ remains unsolved.

From Table VI, it is seen that the PPDP and PTDP chains have almost the same $\lambda^{-1}$ and $M_L$, while the latter chain has an appreciably larger $d$. These results seem reasonable if we take the local contour of the chain in the N–N direction of the piperazine ring in both PPDP and PTDP (see Figure 1 of ref 18). We note that with the model parameters of Table VI, the theory can explain the experimental result that $(\langle S^2\rangle/M)_\infty$ of PTDP is about 1.8 times as large as that of PPDP. Further, note that Motowoka et al.[17,18] determined $d$ from $\bar{v}$, assuming the straight cylinder, but such $d$ are not necessarily identical with the hydrodynamic ones.

**Cellulose Acetate.** We have already analyzed[4] the transport data[19] for cellulose nitrate as the KP chain, for which $\langle S^2\rangle/M$ increases with increasing $M$.[20-22] For some of the cellulose derivatives, however, this ratio decreases with increasing $M$, as pointed out first by Krigbaum and Sperling[23] for cellulose tricaproate. Such cellulose derivatives may possibly be represented by the HW chains.[24] In this paper, we take as an example the data obtained by Tanner and Berry[25] for cellulose acetate (CAc) (degree of substitution 2.45) in TFE at 20 °C. (Note that appreciable intermolecular association has not been found in this system.)

The ratio $\langle S^2\rangle/M$ of this CAc appears to decrease, though slightly, with increasing $M$. However, we regard it as almost independent of $M$, considering the experimental error. Now, suppose that the CAc chain is represented by the KP chain. The constancy of $\langle S^2\rangle/M$ then requires that log $(M_L/\lambda) \lesssim 3.4$. Double logarithmic plots of $\langle S^2\rangle/\langle S^2\rangle_{(C)}$ against $L$ with the data above are shown by the filled circles in Figure 9, where we have taken $(\langle S^2\rangle/M)_\infty$ = 1.15 Å$^2$ and log $(M_L/\lambda)$ = 3.4. The broken curve represents the theoretical values for the KP chain. If log $(M_L/\lambda)$ becomes larger, the filled circles in the figure shift to the left, as seen from eq 55, and the theoretical $\langle S^2\rangle/M$ there increases appreciably with $M$. This is inadequate. We have also found that when log $(M_L/\lambda) \lesssim$ 3.4, the dependence of $[\eta]$ on $M$ requires that $d \leq 0.001$. Double logarithmic plots of $[\eta]$ against $M$ are shown by the open circles in Figure 10, where $M$ is the GPC molecular weight. The broken curve represents the best fit theoretical values calculated as the KP chain with $d$ = 0.001, log $(M_L/\lambda)$ = 3.4, and log $(\lambda^2 M_L)$ = −2.56. From these, we obtain $\lambda^{-1}$ = 97 Å, $M_L$ = 26 Å$^{-1}$, and $d$ = 0.1 Å. These values of $M_L$ and $d$ are too small. Note that the value of $M_L$ corresponding to the full extension of this CAc chain is equal to 50.6 Å$^{-1}$. Thus, the assumption of the KP chain should be rejected.

Next, we assume the HW chain. The full curve in Figure 9 represents the theoretical values of $\langle S^2\rangle/\langle S^2\rangle_{(C)}$ calculated from eq 12 for the HW chain with $\kappa_0$ = 1.96 and $\tau_0$ = 0.4 ($\mu$ = 0.2 and $\nu$ = 2). In this case, it requires that log $(M_L/\lambda) \lesssim 4.3$, and the observed values with log $(M_L/\lambda)$ = 4.3 are shown by the open circles in Figure 9. The full curve in Figure 10 represents the best fit theoretical values of $[\eta]$ for this HW chain with $d$ = 0.014, log $(M_L/\lambda)$ = 4.3, and log $(\lambda^2 M_L)$ = −3.40. We then obtain $\lambda^{-1}$ = 370 Å, $M_L$ = 54 Å$^{-1}$, and $d$ = 5.2 Å. These results seem reasonable. Thus, it is concluded that the CAc chain may be represented by the HW chain, and the radius and pitch of its characteristic helix, as given in Table VI, are relatively large. Such skewness of the chain is probably due to certain configurations of the substituents. There seems to be a similar situation also in cellulose tricaproate.

**Amylose.** It is known that the unsubstituted amylose chain may be regarded as being randomly coiled in aqueous solutions of a simple electrolyte,[26] while its $\langle S^2\rangle/M$ in dimethyl sulfoxide ($Me_2SO$) decreases with increasing $M$.[27-30] Thus, we are interested in the latter system, since it may possibly be represented by the HW chain. However, the data obtained in different laboratories are not always consistent with one another, especially for $[\eta]$. For con-

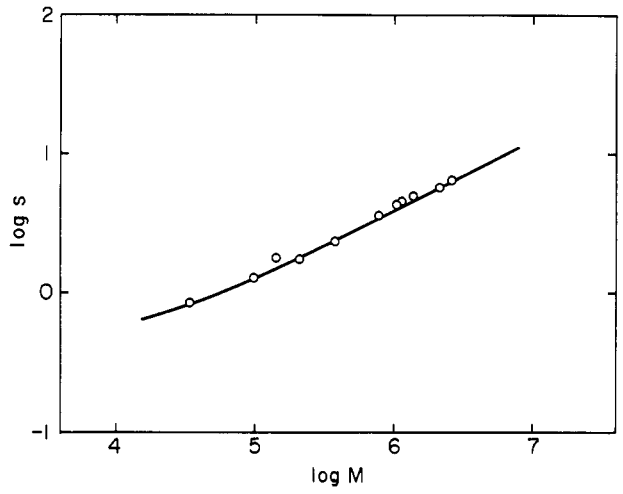


**Figure 11.** Analysis of the data for $s$ for amylose in dimethyl sulfoxide at 25 °C[30] according to eq 54 with eq 55. The curve represents the best fit theoretical values as the HW chain.

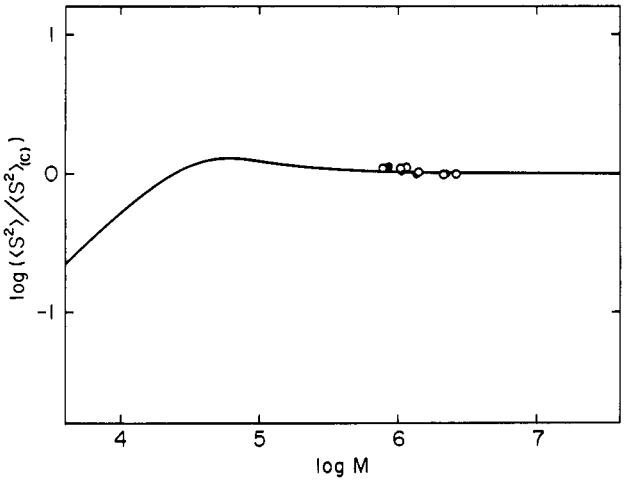


**Figure 12.** Analysis of the data for $\langle S^2 \rangle$ for amylose in dimethyl sulfoxide at 25 °C (open[30] and filled[27] circles) according to eq 59 with eq 55. The curve represents the theoretical values as the HW chain.

venience, therefore, we analyze only the data for $s$ and $\langle S^2 \rangle$ obtained (in $Me_2SO$ at 25 °C) by Fujii et al.,[30] though they are not necessarily accurate.[31] This is daringly done to stimulate further research.

Double logarithmic plots of $s$ against $M$ with these data are shown by the open circles in Figure 11, where $M$ is the weight-average molecular weight. The full curve represents the best fit theoretical values calculated as the HW chain from eq 54 and eq 28 of part 2 with $\kappa_0 = 4.9$, $\tau_0 = 1.0$ ($\mu = 0.2$, $\nu = 5$), $d = 0.02$, $\log (M_L/\lambda) = 4.7$, and $\log M_L = 1.90$. We then obtain $\lambda^{-1} = 630$ Å, $M_L = 79$ Å$^{-1}$, and $d = 12.6$ Å. Double logarithmic plots of $\langle S^2 \rangle / \langle S^2 \rangle_{(C)}$ against $M$ with $(\langle S^2 \rangle / M)_\infty = 0.394$ Å$^2$ are shown in Figure 12, where the data (filled circles) obtained by Everett and Foster[27] are also included. The full curve represents the theoretical values for the HW chain with the same model parameters as above. Thus, the assumption of the HW chain for amylose in $Me_2SO$ is not inadequate. The value of 79 of $M_L$ is intermediate between the value of 122 corresponding to the $V$-type helix of amylose and the value of 32 corresponding to its full extension. (A value of $M_L$ much smaller than 32 is obtained from $s$ if the KP chain is assumed.) This indicates that the crystalline helical conformations are, to some extent, retained in $Me_2SO$ solution. It is important to note that the contour of the continuous chain is taken along the axis of the $V$-type helix where it is, rather than along the actual helical sequence, and that this chain contour itself may also be regarded as having the "helical" nature. The radius and pitch of its characteristic helix, as given in Table VI, are large as in the case of CAc. These conclusions of course require reservation because of the lack of accuracy in the available experimental data.

## Concluding Remarks

We have presented the interpolation formulas for the intrinsic viscosity of helical wormlike cylinders on the basis of the Oseen–Burgers values for long chains and the exact solutions for short spheroid-cylinders. In the case of the translational friction and diffusion (or sedimentation) coefficients, the end effects are rather small, and the formulas presented in part 2 need not be modified. We have shown some salient aspects of the behavior of the intrinsic viscosity in comparison with the sedimentation coefficient. We have also explicitly shown some examples of stiff chains whose configurational and transport behavior may be explained by the helical wormlike chain but not by the ordinary wormlike chain. In general, the radii and pitches of their characteristic helices are relatively large. In other words, the (finite) small radius and pitch cannot be detected from the steady-state transport properties, whose length scales are larger than those associated with the equilibrium chain configurations, as discussed in part 1. Indeed, the conformational behavior of almost all kinds of flexible chains on the bond length or somewhat longer scales may be explained by the helical wormlike chain,[3,32] while the random coil model suffices for an analysis of the steady-state transport properties of long flexible chains. Finally, it is emphasized that a further experimental study of the polysaccharides is required to establish their molecular pictures on the relatively large length scales, though some aspects of the conformational behavior of the discrete chains[33,34] have been clarified. We have just analyzed the data to present the problem.

## References and Notes

(1) Yamakawa, H.; Yoshizaki, T. *Macromolecules* **1979**, *12*, 32.
(2) Yamakawa, H.; Fujii, M. *J. Chem. Phys.* **1976**, *64*, 5222.
(3) Yamakawa, H. *Macromolecules* **1977**, *10*, 692.
(4) Yamakawa, H.; Fujii, M. *Macromolecules* **1974**, *7*, 128.
(5) Yamakawa, H.; Yoshizaki, T.; Fujii, M. *Macromolecules* **1977**, *10*, 934.
(6) Yoshizaki, T.; Yamakawa, H. *J. Chem. Phys.* **1980**, *72*, 57.
(7) Norisuye, T.; Motowoka, M.; Fujita, H. *Macromolecules* **1979**, *12*, 320.
(8) Yamakawa, H.; Shimada, J.; Fujii, M. *J. Chem. Phys.* **1978**, *68*, 2140.
(9) Benoit, H.; Doty, P. *J. Phys. Chem.* **1953**, *57*, 958.
(10) The numerical coefficient 4398.88 in the third term of $C_3$ in eq 39 of ref 4 should be replaced by 43 898.88.
(11) We delete the two values of $\Phi$ for $L = 0.01$ in Table II of ref 4, since their accuracy is not good.
(12) Schlitt, D. W. *J. Math. Phys.* (*N.Y.*) **1968**, *9*, 436.
(13) Taki, N. *Polym. J.* **1975**, *7*, 586.
(14) The theoretical value $2.870 \times 10^{23}$ of $\Phi_\infty$ retained here is the one obtained by solving the integral eq 3 numerically.[4] Its more accurate value obtained recently[15] is $2.862 \times 10^{23}$, which agrees with the Auer–Gardner value.[16]
(15) Shimada, J.; Yamakawa, H. *J. Polym. Sci., Polym. Phys. Ed.* **1978**, *16*, 1927.
(16) Auer, P. L.; Gardner, C. S. *J. Chem. Phys.* **1955**, *23*, 1545, 1546.
(17) Motowoka, M.; Norisuye, T.; Fujita, H. *Polym. J.* **1977**, *9*, 613.
(18) Motowoka, M.; Fujita, H.; Norisuye, T. *Polym. J.* **1978**, *10*, 331.
(19) Meyerhoff, G. *J. Polym. Sci.* **1958**, *29*, 399.
(20) Holtzer, A. M.; Benoit, H.; Doty, P. *J. Phys. Chem.* **1954**, *58*, 624.
(21) Hunt, M. L.; Newman, S.; Scheraga, H. A.; Flory, P. J. *J. Phys. Chem.* **1956**, *60*, 1278.
(22) Schulz, G. V.; Penzel, E. *Makromol. Chem.* **1968**, *112*, 260.
(23) Krigbaum, W. R.; Sperling, L. H. *J. Phys. Chem.* **1960**, *64*, 99.
(24) The decrease in $\langle S^2 \rangle / M$ with increasing $M$ cannot be explained by intermolecular association, since this ratio increases with increasing association according to the estimates of Tan-

ner and Berry (see Table X of ref 25). Note that the association increases with $M$.
(25) Tanner, D. W.; Berry G. C. *J. Polym. Sci., Polym. Phys. Ed.* **1974**, *12*, 941.
(26) Banks, W.; Greenwood, C. T. *Makromol. Chem.* **1963**, *67*, 49. *Carbohydr. Res.* **1968**, *7*, 349.
(27) Everett, W. W.; Foster, J. F. *J. Am. Chem. Soc.* **1959**, *81*, 3459, 3464.
(28) Cowie, J. M. G. *Makromol. Chem.* **1960**, *42*, 230.
(29) Burchard, W. *Makromol. Chem.* **1963**, *64*, 110.
(30) Fujii, M.; Honda, K.; Fujita, H. *Biopolymers* **1973**, *12*, 1177.
(31) Fujita, H. private communication.
(32) Yamakawa, H.; Shimada, J. *J. Chem. Phys.* **1979**, *70*, 609.
(33) Brant, D. A.; Goebel, K. D. *Macromolecules* **1972**, *5*, 536.
(34) Jordan, R. C.; Brant, D. A.; Cesàro, A. *Biopolymers* **1978**, *17*, 2617.

# Viscosity of Solutions of Rigid Rodlike Macromolecules

**R. R. Matheson, Jr.**

*Department of Chemistry, Stanford University, Stanford, California 94305.*
*Received October 24, 1979*

ABSTRACT: The steady flow viscosity of solutions of long, monodisperse, rigid, rodlike macromolecules in good solvents is discussed for the entire range of macromolecular concentrations. It is demonstrated that a proper interpretation of viscosity measurements made over an appropriate concentration range provides important information about the formation of anisotropic phases in such solutions. The concentrations which bound the range of biphasic solution behavior and the mean orientation of the macromolecular rods in an anisotropic (strictly nematic) phase can be evaluated for favorable systems. The sharp maximum in a plot of viscosity vs. concentration is characterized, although it is of only marginal interest in discussions of the isotropic–anisotropic phase transition.

An important group of polymers is composed of macromolecules that adopt the shape of long, rigid rods in appropriate solvents. Above a certain concentration these macromolecules spontaneously form an anisotropic phase, i.e., a liquid crystal. This phenomenon has been explained theoretically[1-3] and observed experimentally by many workers in a variety of systems. An important feature of the transition from isotropic to anisotropic behavior is the concentration of macromolecular rods that is required to induce this phase transition. Many attempts have been made to check the predicted[3] value of this critical concentration by steady flow viscosity experiments. Following the initial investigation of Hermans,[4] it has been the usual practice to identify the characteristic, sharp maximum in a plot of viscosity vs. rod concentration as the harbinger of the onset of anisotropic behavior. The investigation which is reported in this paper was undertaken because such an identification is implausible on physical grounds. However, because the rigid rodlike macromolecules are such an important class of materials, this paper will examine the steady flow viscosity of their solutions over the entire range of rod concentration. The principal focus is directed toward an examination of the utility of steady flow viscosity experiments in elucidating the details of the isotropic–anisotropic phase transition, but simple, physical arguments will also be invoked to clarify the physical basis of the viscosity behavior in the range of concentrations remote from those of biphasic stability.

The systems of interest consist of rigid, rodlike macromolecules dispersed in a good solvent of much lower molecular weight. Typical examples are poly($\gamma$-benzyl glutamate) in *m*-cresol, poly(hexyl isocyanate) in chloroform, and poly(*p*-benzamide) in *N,N'*-dimethylacetamide (all near 300 K). The properties of these and similar systems will be idealized to the extent that they will be modeled as suspensions of identical, inflexible, impenetrable, noninteracting (except for hydrodynamic and steric interactions), and extremely elongated, uniform, cylindrical rods. The steady flow viscosity of such a monodisperse, idealized suspension will be discussed only in the limit of vanishingly small shear rate.

Much of the subsequent analysis recapitulates or stems directly from earlier work by many authors. In the interest of brevity, only specific theoretical papers and a few illustrative experiments which verify their calculations have been cited. The reader is referred to any of the standard texts and review articles on polymer hydrodynamics for a broader perspective, particularly with regard to the subject treated in the Isotropic Regime section. The span of rod concentrations breaks naturally into three regimes, viz., isotropic, biphasic, and wholly anisotropic solutions. Each is considered in turn.

## Isotropic Regime

Let $\eta_{sp}$ denote the specific viscosity of an isotropic suspension of macromolecules. In general, an equation of the form

$$\eta_{sp} = \nu_e\varphi + k_1(\nu_e\varphi)^2 + k_2(\nu_e\varphi)^3 + k_3(\nu_e\varphi)^4 + \ldots \quad (1)$$

is appropriate.[5,6] Here $\varphi$ is the volume fraction of polymer, $\nu_e$ is a coefficient which depends on the shape of the macromolecule (the so-called Einstein coefficient), and $k_1$, $k_2$, etc., are coefficients which are at most slowly varying functions of molecular shape.[7] For rigid rods $k_1$ is 0.73 according to Riseman and Ullman[8] and 0.77 according to Simha.[9] An averaged value of 0.75 was verified (approximately) by Hermans.[4] For sufficiently elongated, prolate ellipsoids of revolution $\nu_e$ will be specifically denoted $\nu$. It is given as[10]

$$\nu = \frac{J^2}{15}\left(\frac{1}{\ln 2J - 1.5} + \frac{3}{\ln 2J - 0.5}\right) + \frac{14}{15} \quad (2)$$

where $J$ is the axial ratio of the ellipsoid ($J \gtrsim 15$). This well-known expression is applicable to cylindrical rods of length $L$ and diameter $d$ if $J$ is replaced by $(L/d)(2/3)^{1/2}$.[11] Since the sole interest of the subsequent discussion is with such rods, eq 2 is explicitly recast as

$$\nu = \frac{2x^2}{45}\left(\frac{1}{\ln 2x - 1.8} + \frac{3}{\ln 2x - 0.8}\right) + \frac{14}{15} \quad (2a)$$

where $x$ is the axial ratio of the rods ($x = L/d \gtrsim 19$).

0024-9297/80/2213-0643$01.00/0 